https://doi.org/10.5194/wes-2025-85
Preprint. Discussion started: 25 June 2025

Methods for Pacific Outer Continental Shelf Wind Characterization for Offshore Wind Development

Macy Frost Chang[1], Raghavendra Krishnamurthy[2], and Fotini Katopodes Chow[1]

[1]Civil and Environmental Engineering, University of California, Berkeley, California, USA
[2]Pacific Northwest National Laboratory, Washington, USA

Correspondence: Fotini K. Chow (tinakc@berkeley.edu)

Abstract. The rapid development of the U.S. offshore wind industry has necessitated accurate assessment and prediction of offshore wind profiles to manage and forecast generated power. In 2021, the Bureau of Ocean Energy Management (BOEM) identified two areas on the Pacific Outer Continental Shelf (OCS), the Humboldt and Morro Bay Wind Energy Areas (WEAs), as potential locations for offshore wind farms. Although these areas have historically lacked high-quality observations of wind characteristics at typical wind turbine hub heights, scientific buoys sponsored by the Department of Energy and deployed by the Pacific Northwest National Laboratory (PNNL) recently made precise hub-height wind data available for the first time in these locations, introducing novel opportunities for model validation and intercomparison. Performances of 100-meter AMSL wind speed prediction are compared between a conventional physical law-based approach, known as the stability-corrected logarithmic law (S-C log law), and three machine learning (ML) approaches, known as random forest (RF), Guassian process regression (GPR), and long short-term memory neural network (LSTM). Predictor variables for the ML approaches are constrained to only sea surface-elevation measurements, and the ML algorithms are respectively trained and tested between the two separate locations (over a notable extrapolation distance of 631 kilometers) in order to simulate realistic industry applications and preclude model overfitting from biasing performance metrics. The S-C log law and LSTM produce the most accurate predictions, with average root mean squared error (RMSE) of 1.33 m/s and 1.38 m/s respectively. The error metrics of all three ML methods generally improve when a longer training time is implemented and when the algorithms are trained and tested at the same location, with many performance metrics of LSTM surpassing those of the S-C log law. The LSTM and GPR techniques overall exhibit similar or improved offshore wind speed prediction capabilities in comparison to the S-C log law, which is a widely accepted wind speed extrapolation method. These ML techniques are more adaptable for wind energy purposes than conventional physical extrapolation laws, as they can be used to predict other wind parameters and generate short-term forecasts. The increasing future availability and fidelity of vertical wind profile data from the Pacific OCS will be vital for determining the degrees of ML performance degradation over smaller train-test distances and for evaluating performance and power output metrics of larger offshore turbines.

https://doi.org/10.5194/wes-2025-85
Preprint. Discussion started: 25 June 2025

1 Introduction

Wind energy is a renewable energy technology that is continuing to rapidly expand and evolve across the globe. Wind energy generation has grown by approximately 15% annually over the past decade, making it the current largest source of renewable energy in the United States ESMAP. With record installations of wind turbines worldwide in 2023, global wind power capacity has surpassed 1 terawatt and currently supplies approximately 10% of global electricity demand WWEA (2024). Recent technological advances and stakeholder interest are allowing new areas to become feasible for wind farm construction. Bottom-mounted and floating wind turbine structures allow for construction and operation of wind farms in offshore locations, where wind speeds tend to be higher and more consistent than over land Wang and Wang (2015). The U.S. Bureau of Ocean Energy Management (BOEM) has approved several wind energy lease areas along the Atlantic Coast. Three offshore wind sites on the Atlantic coast are already in operation and demonstrate the economic and energetic feasibility of offshore wind energy siting (BOEM, 2025).

Sections of the Pacific Outer Continental Shelf (OCS), the area of ocean extending to about 200 nautical miles from the U.S. West Coast, have recently come into consideration for offshore wind development. In May of 2021, plans were announced to develop floating offshore wind farms in two Pacific OCS locations off the coast of Morro Bay and Humboldt County, which together have the potential to provide up to 4.6 GW of electricity, equivalent to powering 1.6 million homes Release (2021). These two locations were titled as “Wind Energy Areas” (WEAs) by BOEM after collaborating with federal agencies, the state of California, local tribes and communities, and the public to consider potential impacts on the environment as well as ocean resources and commerce. In 2022, the WEAs were split into five subareas for lease and auctioned off to private developers McCoy et al. (2024).

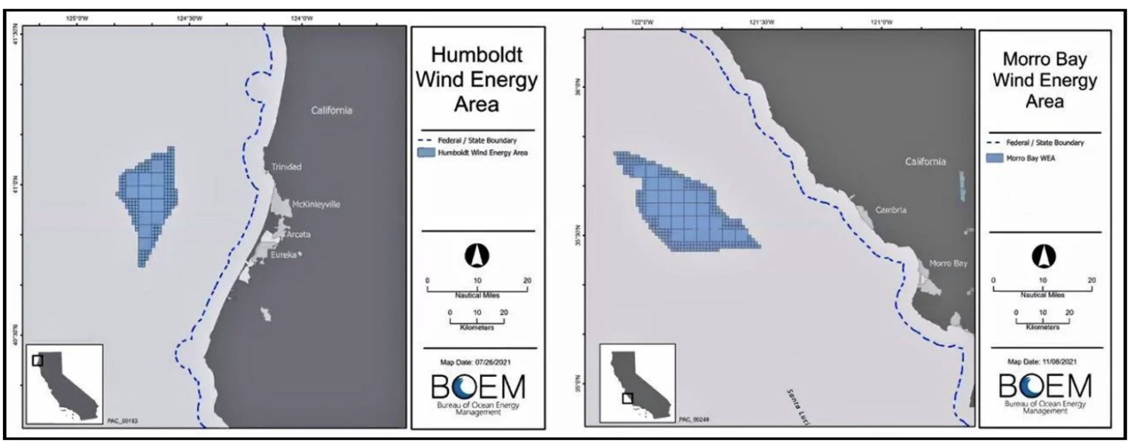

Figure 1. The geographic areas of the Humboldt and Morro Bay Wind Energy Areas (WEAs) identified by the U.S. Bureau of Ocean Energy Management. (Images adapted from BOEM.gov, BOEM (a, b))

https://doi.org/10.5194/wes-2025-85
Preprint. Discussion started: 25 June 2025

eawe european academy of wind energy
Open Access WIND ENERGY SCIENCE DISCUSSIONS

Along the U.S. West Coast, the impact of atmospheric and oceanographic conditions on offshore wind turbines is largely unknown. Due to the sharp gradient in the bathymetry of the seafloor extending from the coastline, future wind farms will primarily be composed of floating offshore wind turbines. Furthermore, existing high-resolution models for estimating the wind resource are challenged by complex wind-wave-terrain interactions, large amounts of cloudiness, and shallow atmospheric boundary layers typically observed in this region. Therefore, the development of offshore wind farms requires extensive research of atmospheric and oceanographic factors that affect wind farm layout, predicted power output, and fatigue load estimations. Until recently, only a few sea surface-monitoring buoys scattered along the Pacific OCS have provided direct observational data of offshore meteorological and oceanic characteristics. These buoys measure only surface variables and do not provide vertical profiles of winds and turbulence throughout the surface atmospheric boundary layer (ABL), which is critical information needed by wind energy developers.

As of September 2020, a research campaign funded by BOEM and the U.S. Department of Energy (DOE) has made direct, consistent observations of above-surface wind characteristics in the Pacific OCS available for the first time. The Pacific campaign consisted of two specialized research buoys stationed in the Humboldt and Morro Bay WEAs. These buoys measure wind speed and direction up to 250 meters above mean sea level (AMSL) as well as a large set of surface variables (Krishnamurthy et al., 2023). This data can be used to assess the wind resource at potential turbine heights in these Pacific OCS sites. It also introduces new possibilities for validating wind prediction models in the Pacific OCS region. More specifically, the observational data is vital for identifying model biases and optimizing the performance of statistical, physical, and intelligent learning wind prediction methods Shao et al. (2021); Sheridan et al. (2024); Liu et al. (2024); Bodini et al. (2024).

New strategies for wind speed extrapolation from sea surface-elevation data could prove to be more adaptable and site-specific than relatively complex and computationally-expensive numerical weather prediction (NWP) models (de Montera et al., 2022). Additionally, improved wind modeling accuracy and new intelligent modeling approaches may help to enhance confidence in turbine and wind plant power production estimates, which would have significant impacts on downstream analyses, including grid integration and expansion Ortega et al. (2020); Mahoney et al. (2012); Hasager et al. (2015) as well as life-cycle cost analyses of floating offshore wind energy production Jong et al. (2017). At both California WEAs, reanalysis data consistently falls short in capturing the full potential of the rotor-level wind resource (Sheridan et al., 2022). The most significant errors arise during stable atmospheric conditions, when wind speeds surpass 10 m/s, which is critical for peak turbine power generation, and when diurnal the wind speed variation in summer months is poorly represented, leading to substantial errors in estimation of wind energy potential (Sheridan et al., 2024). Considering the recency of the collected Pacific OCS wind data, an imminent research need is to test out different wind prediction models and assess which techniques provide the best wind estimates for energy developers (Gaudet et al., 2024; Liu et al., 2024, 2025).

A large suite of wind prediction techniques are in use by the wind industry and could potentially be tested in these offshore areas. One category of techniques is physical modeling, wherein meteorological variables are input into physical law equations to calculate other weather characteristics (Fairall et al., 1996; Edson et al., 2013). Another contemporary group of techniques are intelligent learning methods, which most often use machine learning (ML) architecture to draw complex statis-

https://doi.org/10.5194/wes-2025-85
Preprint. Discussion started: 25 June 2025

tical relationships between input data and subsequently make predictions (Crippa et al., 2021; Optis et al., 2021; Vassallo et al., 2020a).

In this study, prediction methods from both of these categories are tested by comparing their accuracy and adaptability across the Humboldt and Morro Bay WEAs. The hub-height wind characteristics are analyzed to find relationships between these hub-height winds and surface variables, where “hub height" is generalized as 100 AMSL for this study, but could be extended to any height to match newer offshore turbine sizes. These relationships are drawn from analyzing correlations of 100-meter AMSL winds to surface wind speed, air and sea temperature, atmospheric pressure, and temporal characteristics. The primary goal is to compare vertical wind extrapolation performance of a widely-used physical law approach, the stability-corrected logarithmic law (denoted as S-C log law), versus the machine learning methods of random forest (RF), Gaussian process regression (GPR), and long short-term memory neural network (LSTM).

The three aforementioned ML algorithms were selected for this study due to their varied advantages and shortcomings for wind profiling purposes. RF effectively handles missing values, nonlinear parameters, and outlier data, though its stable nature may limit its effectiveness in capturing stochastic variability in time series data. GPR also handles missing and nonlinear data well and provides confidence intervals for predictions, but the computational intensity required by its nonparametric design may limit efficiency for large datasets. LSTM has demonstrated high accuracy for wind speed prediction due to its specific design for retaining long-term patterns in time series data, but it requires more hyperparameter tuning to each specific use case as well as complete datasets. To the authors' knowledge, these three ML algorithms have not been compared within one wind speed prediction study. Additionally, applications of these algorithms to the Pacific OCS wind resource are sparse due to the historical data limitations and previous lack of research motivation.

Comparison of these ML algorithms against a standard physical law-based approach offers new insights into the most suitable current methods for Pacific OCS wind speed prediction. The ML models are developed by training on one buoy's sea surface-elevation data and testing using the other buoy's data to minimize training location bias and assess the adaptability of each ML algorithm to other offshore locations (Bodini and Optis, 2020). This style of testing helps gauge the greater applicability of these ML methods to other Pacific OCS offshore areas where meteorological data are only available at the sea surface elevation.

2 Methods

2.1 Source Data

Data from the DOE/PNNL lidar buoys is retrieved from the Atmosphere to Electrons Data Archive and Portal, which is supported by the U.S. Department of Energy, Office of Energy Efficiency and Renewable Energy's Wind Energy Technologies Office. The data is publicly available at a2e.energy.gov DOE (2021); Krishnamurthy et al. (2023). All analysis performed in this study uses 10-minute averaged data. For the Humboldt WEA, the data included in this analysis span from October 2020 to January 2022. Due to instrument failure from the end of December 2020 through May 2021, the Humboldt buoy was deployed until July 2022 in order to retrieve a full annual cycle of wind data, but data following January 2022 was not obtained before

https://doi.org/10.5194/wes-2025-85
Preprint. Discussion started: 25 June 2025

the completion of this study. The Morro Bay buoy provides mostly continuous data coverage from September 2020 to October 2021.

The motion-corrected Doppler lidar data were filtered for appropriate signal-to-noise ratios of less than -23 dB. The remaining values are not expected to fall outside of instrument technical specifications of ± 0.1 m/s wind speed accuracy and $\pm 2°$ wind direction accuracy Vaisala. Standard filtering thresholds were also applied to the surface-monitoring and in-situ sea surface measurement instruments (Krishnamurthy et al., 2023).

The predictor features were selected based on analysis of surface variable correlations to 100-meter AMSL wind speed and are listed in Table 1. Time of day is cyclically encoded into cosine and sine components for use by the ML algorithms. This transformation creates a polar representation of time to reduce the numerical difference in magnitude between different parts of the day, while also maintaining continuity between consecutive hours of the day. An important drawback of this transformation is that the sine and cosine components must be considered together to identify a unique time of day. Thus, algorithms which handle only one input feature at a time may deflate the overall predictive power of the encoded time features.

Predictor Feature	Unit	Measurement Height (m AMSL)
Surface Wind Speed	m/s	4
Air Temperature	°C	3.7
Sea Surface Temperature	°C	0
Air-Sea Temp. Difference	°C	-
Atmospheric Pressure	mbar	~ 1
Time of Day (cosine)	-	-
Time of Day (sine)	-	-

Table 1. Input feature variables used for ML training and prediction of 100-meter AMSL wind speed.

Considering the frequency of missing or filtered buoy data which resulted in many data gaps spanning more than a day, the selection of train-test datasets was conducted based on the following criteria:

- Parallel day-of-year data availability at both Humboldt and Morro Bay sites
- Approximately one month-long continuous data, with no longer than one continuous day of missing data for any variable
- No data overlap with other train-test datasets

The data selection based on the above criteria resulted in six datasets, detailed in Table 2. Because of the limited data availability, assessment of the ML algorithms' longer-term wind speed prediction capabilities over variable seasonal conditions is not included in this analysis.

https://doi.org/10.5194/wes-2025-85
Preprint. Discussion started: 25 June 2025

Dataset Month Range	Dates (Month/Day)	No. of Days
October	10/01 - 10/31	31
November	11/01 - 11/30	30
December	12/01 - 12/28	28
January	01/01 - 01/23	23
June	06/01 - 06/30	30
July-August	07/12 - 08/04	23

Table 2. Train-test dataset ranges, selected for data completion and continuity.

Within the selected datasets, 2.1% of Humboldt and 1.5% of Morro Bay data remain sporadically missing. Missing values were filled using the mean hourly value within the month containing the missing value. Though random forest and Guassian process regression do not technically require fully-complete datasets, the same filled datasets are used for all ML methods due to the complete-data requirement of LSTM. The first 80% of data in each dataset is used for model training, with the remaining 20% used for testing. The 10-minute data is averaged hourly for faster overall computation time.

Prior to ML algorithm training, input features are scaled through transformation to a standardized z-score in order to prevent features with wider ranges from exerting more influence on the target prediction. Standardization is performed using the StandardScaler function from the scikit-learn *preprocessing* module. After data are scaled, principal component analysis (PCA) is used to reduce the dimensionality of the input data. PCA is performed using the scikit-learn *PCA* module with a lower variance threshold of 0.95, meaning at least 95% of original dataset variance is captured by the modified features.

2.2 Hub-height Wind Characteristics

Frequency distributions of hub-height (100 meters AMSL) wind speeds in both WEAs are shown in Figure 2. Wind speeds at hub-height in these areas average around 8-10 m/s, with strong gusts reaching 25-30 m/s. These wind speed attributes are desirable to wind energy developers, as the technically viable lower limit for 100-meter AMSL offshore wind speeds is 7 m/s for the current performance standards of offshore wind turbines ESMAP and the cut-out speed is roughly 25 m/s. The Weibull distribution shown in Figure 2 is fit to each dataset using the maximum likelihood method, but the mismatch with the data demonstrates that more sophisticated methods are necessary to accurately model even general hub-height wind characteristics in these areas.

Average hub-height wind direction is obtained from the lidar data and shown in Figure 3. Hub-height winds hail predominantly from the north in the Humboldt WEA and from the northwest in the Morro Bay WEA. The occurrences of wind direction reversal, visible in the Humboldt windrose, take place in October through December, though other aspects of the seasonal wind direction pattern may be missing due to the data gap from February through May.

The lidar instrument data from 40 to 250 meters AMSL provides surface ABL wind speed profiles across seasonal timescales. The profiles displayed in Figure 4 were created using a 30-day window rolling average of wind speeds at each elevation. The

https://doi.org/10.5194/wes-2025-85
Preprint. Discussion started: 25 June 2025

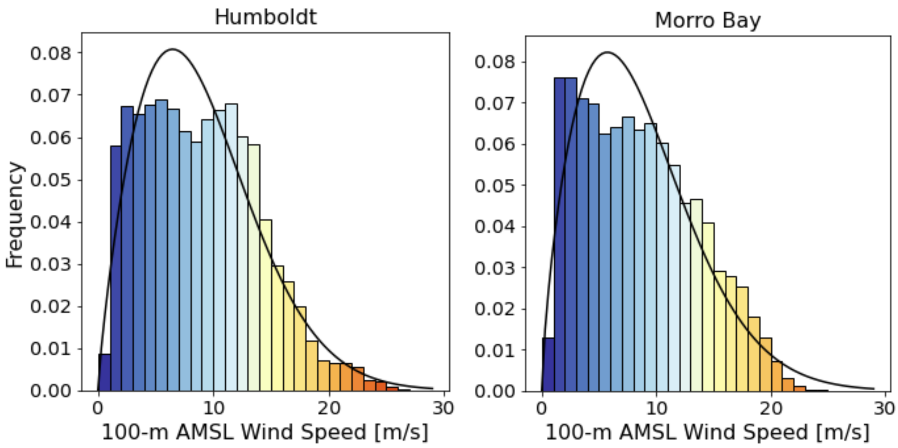

Figure 2. 100-meter AMSL wind speed frequency distributions in the Humboldt and Morro Bay WEAs, based on Humboldt lidar data from October 2020 to January 2022 (with data missing February through May 2021) and Morro Bay lidar data from September 2020 to October 2021.

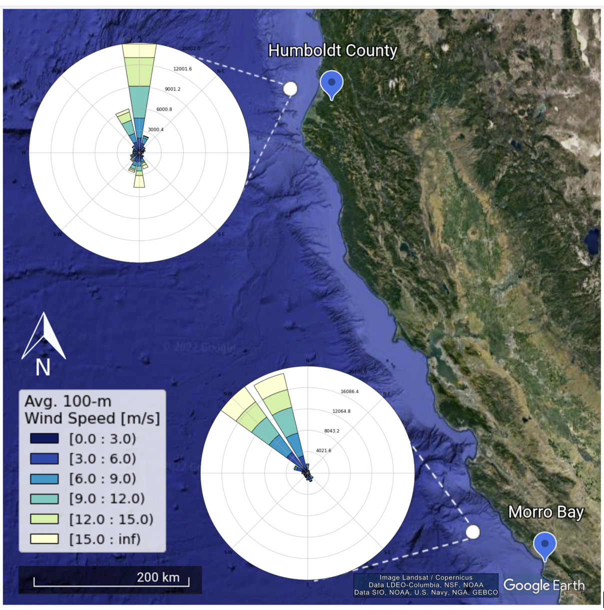

Figure 3. 100-meter AMSL wind direction distributions in the Humboldt and Morro Bay WEAs. The dates of the source data are the same as Figure 2 above. (Satellite imagery adapted from © Google Earth).

https://doi.org/10.5194/wes-2025-85
Preprint. Discussion started: 25 June 2025

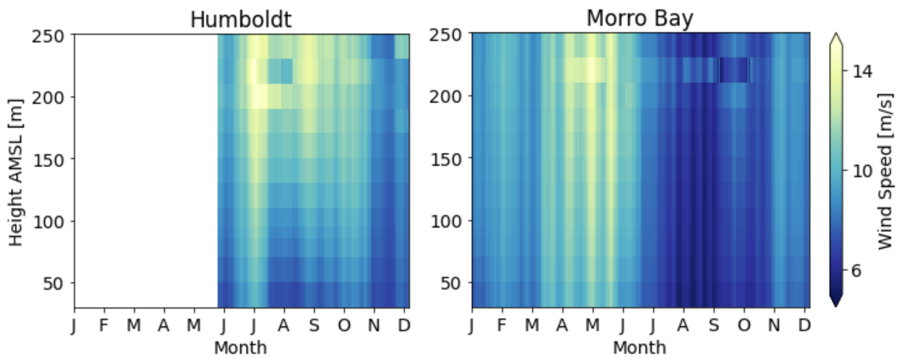

Figure 4. Average interseasonal wind speed profiles from 40 to 250 meters AMSL in the Humboldt and Morro Bay WEAs. The dates of the source data are the same as Figure 2 above, with data wrapped around across years and January not shown for Humboldt.

irregular signatures appearing above 175 meters may be due to a higher ratio of missing data at these heights. Less consistent data at higher elevations is an inherent drawback of lidar wind monitoring, as signal-to-noise ratios from these heights are more likely to be of lower quality and result in data infidelity.

Clear seasonal signatures of increased wind speed occur in springtime months at the Morro Bay site, with the subsequent profile minima occurring in the summertime months. The seasonal wind speed profile variation in Humboldt is less clear due to the large volume of missing data, but the available data does not exhibit seasonal similarities to Morro Bay.

Machine learning algorithms used for time-series data prediction may overfit to long-term patterns within the training data, resulting in reduced prediction accuracy when applied in other locations where similar patterns are not present. The differing seasonal wind speed patterns between the two WEAs thus raise a potential issue for training and applying the ML models across the two locations. The ML models in this study are likely less prone to these types of errors due to the short-term training datasets, which reduce the influence of meteorological patterns present across interseasonal timescales. This consideration is more important for future studies of the Pacific OCS wind resource that may use multiseasonal data from one location to perform wind prediction or forecasting at another location.

2.3 Atmospheric Stability Calculations

2.3.1 Stability Classification

Categorization of atmospheric stability conditions throughout the data collection period is important for identifying conditions in the ABL that correlate with greater model uncertainty or error. The dimensionless height parameter, z/L, was obtained from bulk Richardson number (RI_B) calculations and application of Monin-Obukhov stability theory (Grachev and Fairall, 1997). Further details are given in Chang (2022). This methodology is hereafter referred to as the “profile method”. z/L approaching zero indicates neutral atmospheric conditions, while positive and negative values indicate more stable or unstable, respectively.

https://doi.org/10.5194/wes-2025-85
Preprint. Discussion started: 25 June 2025

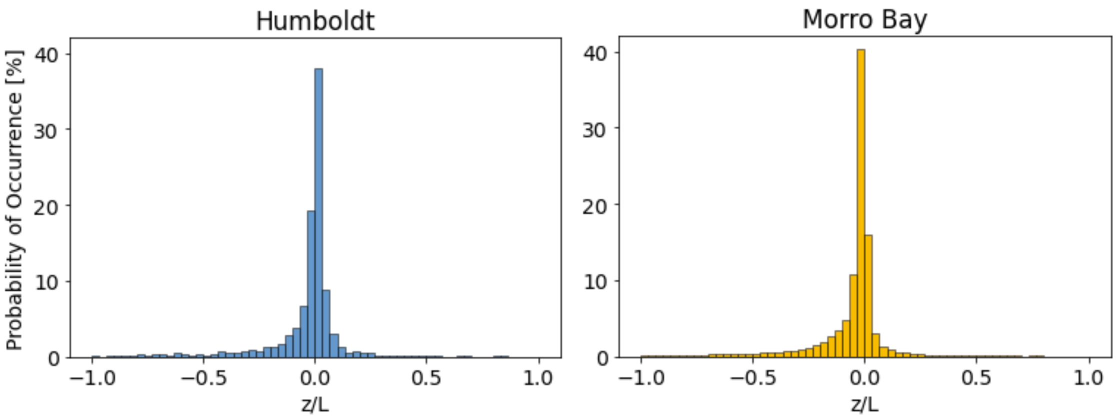

Figure 5. Probability distributions of calculated z/L using the "profile method". Calculations are based on all available, complete 10-minute data from October 2020 through January 2022.

Figure 5 shows the z/L probabilities from each 10-minute averaged data point over the entire deployment period. Both probability distributions exhibit a slight negative skew, indicating a relatively higher ratio of unstable conditions to stable conditions in both locations.

Stability conditions can be labeled by respective Obukhov length L for each time point, as categorized in Table 4.3 of Chang (2022). Percentages of data in each atmospheric stability class are given in Table 3. Both the Humboldt and Morro Bay WEAs primarily experience unstable atmospheric conditions. The Morro Bay ratios are more meaningful as they represent a full year of nearly complete data, while the Humboldt data may exert inherent bias toward summertime and autumnal conditions given the absence of data from February through May.

Chang (2022) includes comparisons of stability calculations with those from the COARE algorithm, a more sophisticated approach relying on additional meteorological variables. Overall, the stability classification using the profile method agrees well with the results from COARE, with a small skew of the Profile Method toward unstable conditions. The profile method is therefore used in further atmospheric stability analysis for simplicity.

Study Location	**% Unstable**	**% Neutral**	**% Stable**
Humboldt	46.8	20.1	33.1
Morro Bay	59.4	24.1	16.5

Table 3. Percentage classification of atmospheric stability conditions in the Humboldt and Morro Bay WEAs. The classification scheme, based on the value of Obukhov length L, is detailed in Table 4.3 of Chang (2022).

https://doi.org/10.5194/wes-2025-85
Preprint. Discussion started: 25 June 2025

2.4 Physical Law Calculations

2.4.1 Stability-Corrected Logarithmic Law

The physical law extrapolations of wind speed are conducted using the stability-corrected logarithmic law, denoted as S-C log law. The logarithmic profile describes the vertical distribution of mean horizontal wind speeds within the surface layer of the ABL, which typically ranges up to 100 meters above the surface during the day or approximately 10% of the boundary layer depth Geernaert (2003). The stability-corrected logarithmic wind profile can be written as:

$$U(z) = \frac{u_*}{\kappa}\left[\ln\left(\frac{z}{z_0}\right) - \psi_m\left(\frac{z}{L}, \frac{z_0}{L}\right)\right] \tag{1}$$

where U is the horizontal wind speed at height z above the surface, u_* is the friction velocity, κ is the von Kármán constant (0.4), z_0 is the surface roughness, ψ_m is the universal stability function for momentum, and L is the Obukhov length, with further details in Chang (2022).

The friction velocity u_* is a dynamic fundamental scaling velocity derived from surface stress and air density measurements. A sonic anemometer instrument is typically used to capture fine-scale wind speed fluctuations in order to calculate the friction velocity. However, the longitudinal and vertical wind speed fluctuation data measured by the 2D ultrasonic anemometers on lidar buoys is not publicly available. Therefore, the above equation is reformulated into a modified logarithmic law, in which the wind speeds at the buoy sea surface-monitoring height are used as a reference measurement:

$$U(z) = U_{4m}\left[\frac{\ln\left(\frac{z}{z_0}\right) - \psi_m\left(\frac{z}{L}, \frac{z_0}{L}\right)}{\ln\left(\frac{z_{4m}}{z_0}\right) - \psi_m\left(\frac{z_{4m}}{L}, \frac{z_0}{L}\right)}\right] \tag{2}$$

where U_{4m} is the horizontal wind speed at 4 meters above mean sea level and z_{4m} is equal to 4 meters, the height above mean sea level of the buoy's cup anemometer and wind vane.

The surface roughness z_0 is typically determined empirically using the friction velocity. Other methods to estimate z_0 without empirically-derived friction velocity exist, such as analytical methods of the COARE model Fairall et al. (1996); Grachev and Fairall (1997) or statistical methods using data from multiple vertical wind measurement points Golbazi and Archer (2020) or using the height and steepness of the waves Taylor and Yelland (2001). However, the former case involves computationally-intensive iterative calculations and a large suite of input parameters, some of which are not publicly available or reliably measured from the Pacific OCS buoy deployments. In the latter case, there is a need for multiple vertical measurement points throughout the surface layer, which does not meet the study's practical constraint of only using sea surface-elevation measurements as input data.

With these considerations, calculations for atmospheric stability and logarithmic wind profiles are simplified and subsequently cross-referenced with COARE 3.6 outputs. Instead of the iterative solving used in the COARE algorithm, surface roughness is characterized according to the Davenport roughness classification of z_0 = 0.0002 m for sea surface with fetch

https://doi.org/10.5194/wes-2025-85
Preprint. Discussion started: 25 June 2025

greater than 3 kilometers. Roughness lengths of this classification scheme have been well-studied and reassessed Wieringa (1992), and this sea roughness parameter is used commonly in related offshore atmospheric stability studies Barthelmie et al. (2007); Lange et al. (2004); Dhiman and Deb (2020).

2.5 Machine Learning Techniques

All ML algorithms are trained on one location and tested on the other (i.e. Morro Bay WEA wind speed predictions are made from an ML model trained on Humboldt WEA data, and vice versa), unless otherwise stated. This method is used to eliminate model bias to the same train-test location and to simulate a realistic application of the model to a different location.

2.5.1 Random Forest

Random forest (RF) is one of the most commonly-used ML algorithms across the field of data science. It is a supervised ensemble ML technique, meaning that it uses labeled data and aggregates multiple submodels to make predictions. In this case, the submodels are decision trees, which work by finding the optimal binary splits in input data to generate the most accurate possible prediction of the output. In the case of continuous input data, such as the meteorological and oceanic DOE buoy data, the decision trees are often called “regression trees". The RF algorithm constructs independent regression trees to subsets of the training data, then aggregates these weak predictions into a more accurate, overall prediction Vassallo et al. (2020b). The features used for splitting include 4-meter AMSL wind speed, sea surface temperature, air temperature, and air-sea temperature difference.

Random forest regression is performed using the *RandomForestRegressor* module from the scikit-learn Python machine learning library. 3-fold grid search cross validation is used to determine the optimal hyperparameter values of the RF model for each train-test dataset. The range of values considered for each hyperparameter is shown below in Table 4.

RF Hyperparameter	Range of Values
Number of estimators (trees)	10 - 1000
Maximum depth	4 - 40
Max number of features considered at a node	2 - 6
Min number of samples to split a node	2 - 10
Min number of samples at each end node	1 - 15

Table 4. Hyperparameters optimized in each training run of random forest regression.

2.5.2 Gaussian Process Regression

Similar to RF, Guassian process regression (GPR) is a supervised ML method used widely for both regression and classification problems. Unlike the traditional RF model, GPR is probabilistic in that it calculates a probability distribution over the

https://doi.org/10.5194/wes-2025-85
Preprint. Discussion started: 25 June 2025

prediction, lending GPR the powerful advantage of quantifying empirical uncertainty over all of its predictions Rasmussen and Williams (2008). GPR defines a mathematical distribution over all the possible functions that can fit some observed data points. Hyperparameters within the radial basis function (RBF) kernel used for this model include vertical scale (the values that the averaged function can span) and horizontal scale (the strength of correlation between two points as distance between them increases). Other hyperparameter specifications include the mean of the prior distribution (either zero or the training data mean) and allowable noise level in the targets. The empirical confidence intervals in areas of interest allow the user to decide if or how the prediction should be refit.

Guassian process regression is performed using the *GaussianProcessRegressor* module from the scikit-learn Python ML library. All input values are normalized by mean removal and scaling to unit variance to ensure that the Gaussian assumptions of GPR are met. An additive kernel consisting of RBF and noise kernels is used. The smoothness of the output function, defined by the RBF length scale ℓ, is optimized within the bounds (1e-2, 1e3) with an initialization value of 0.1. The noise level is optimized within the bounds (1e-15, 1e5) with an initialization value of 0.1^2.

2.5.3 Long Short-Term Memory Neural Network

Long short-term memory (LSTM) neural networks were introduced in 1997 by Hochreiter and Schmidhuber Hochreiter and Schmidhuber (1997) as an advanced type of recurrent neural network (RNN) to more effectively model long-term dependencies. RNNs are still a widely used machine-learning method for modeling of dynamic temporal data Moon et al. (2019). LSTM is state-of-the-art neural network architecture that captures patterns with long-term dependencies within time series data, which RF and GPR are not specifically designed to handle. A disadvantage of LSTM is the need for complete training and testing datasets at regular time intervals. Adverse weather conditions and instrument failure make missing values a common occurrence in wind measurement data, meaning that missing data must be filled in order to use LSTM.

LSTM is implemented here using modules from the Keras Python library with a Tensorflow backend. A stacked LSTM with four layers is used to increase levels of abstraction to the input data, essentially creating representations of the data at different timescales. A dropout algorithm with a rate of 0.2 is applied to randomly omit 20% of each layer's information to help prevent overfitting. Mean absolute error (MAE) is used as the loss function, and the Adam optimization algorithm, which is an efficient method of stochastic gradient descent, is used as the optimizer. 200 epochs and a batch size of 72 are used for iteration over the dataset, which were determined by empirical observations of the loss function and runtime.

3 Results & Analysis

3.1 Prediction Performance & Comparison

3.1.1 Variable Importance

Random forest provides a measure of variable importance (VI) by calculating the increase in mean square error (MSE) when each input variable is randomly permuted. Figure 6 illustrates that the significant majority of prediction power is sourced from

https://doi.org/10.5194/wes-2025-85
Preprint. Discussion started: 25 June 2025

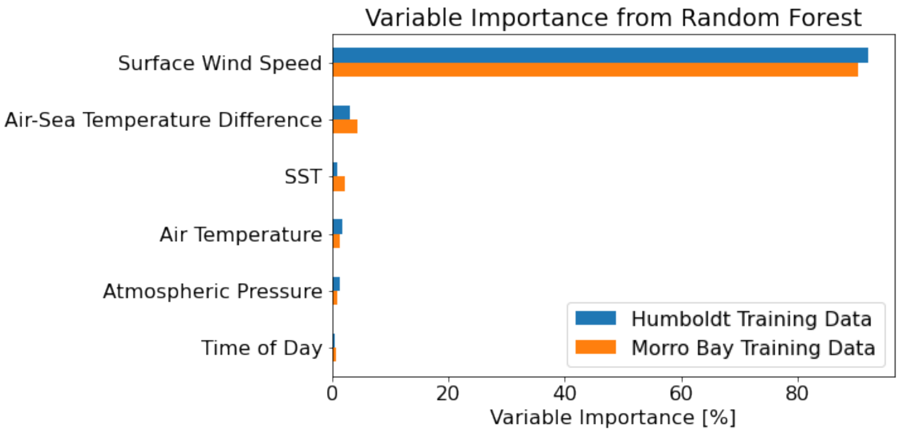

Figure 6. Variable Importance (VI) of each input feature, calculated automatically via random forest regression.

the 4-meter AMSL wind speed, exerting over 90% VI. Out of the three temperature parameters, air-sea temperature difference demonstrates more predictive power than the values of air temperature or sea surface temperature (SST) alone.

Despite a clear diurnal signature of 100-meter wind speed for most months of the year (see Figure 5.9 of Chang (2022)), the combined sine and cosine components of the time of day exert the least predictive power out of all considered features. This result does not mean that time of day is insignificant in predicting the hub-height wind speed. It is likely that RF inherently reduces the importance of the time of day sine and cosine components (which encode unique times of the day only when considered together) because the regression trees split only one feature at a time. It is also possible that the 100-meter wind speed pattern correlated to the time of day may be more precisely encoded by the pattern of near-surface wind speed and/or air-sea temperature fluctuations.

The obtained VI implies that the S-C log law utilizes the two most important parameters (surface wind speed and air-sea temperature difference) for extrapolating hub-height wind speeds from surface measurements. This importance is relative to the seven predictors considered in this study and omits an exhaustive search of other possible predictor variables, such as significant wave height, surface current strength, and wind direction. The following assessment and intercomparison of model performances demonstrate the sufficiency of using only these seven features to obtain accurate predictions of 100-meter AMSL wind speed.

3.1.2 ML Prediction Samples

Across all three ML method hub-height wind speed predictions, the hourly fluctuations and multi-day trends of hub-height wind speed are well represented. The relative accuracy of each model over these dates is not easily inferred due to the varying lengths and instances of prediction inaccuracies between the three methods. Figure 7 visualizes samples of each algorithm's performance on the same subset of testing data.

https://doi.org/10.5194/wes-2025-85
Preprint. Discussion started: 25 June 2025

WIND ENERGY SCIENCE DISCUSSIONS

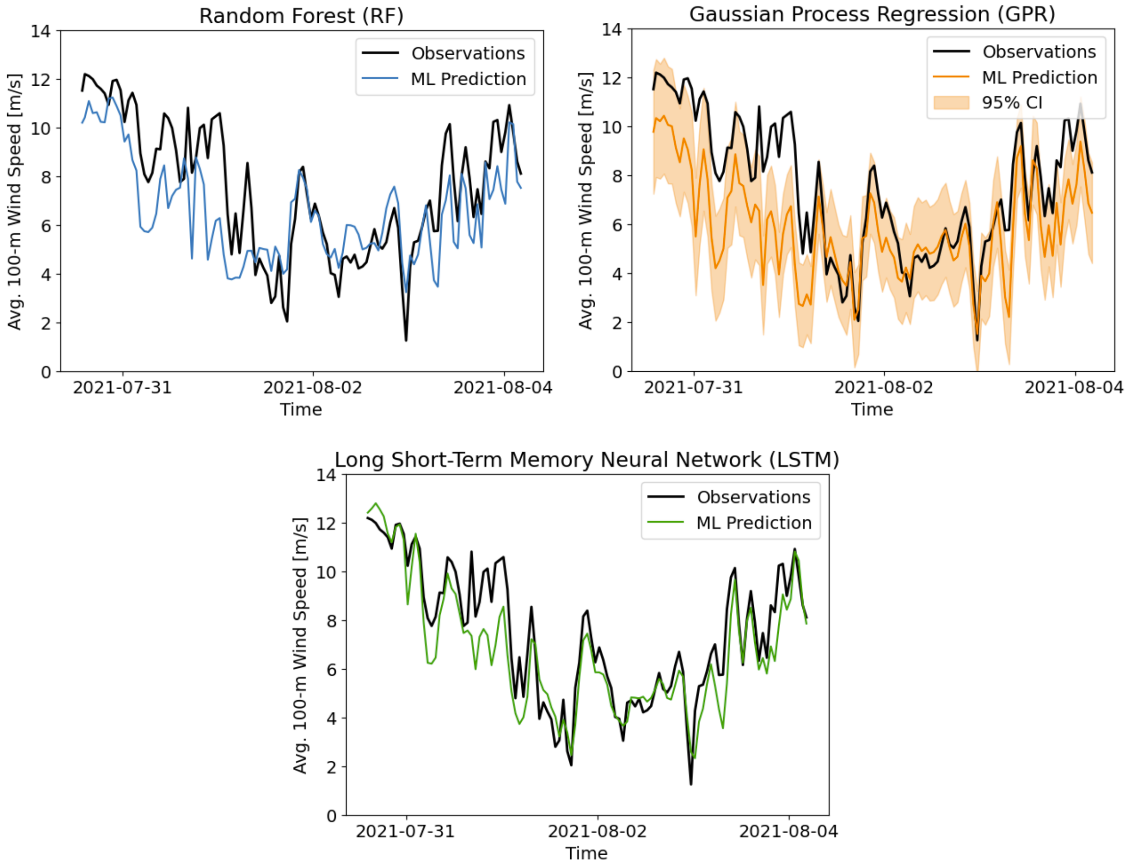

Figure 7. Samples of ML predictions of 100-meter AMSL wind speeds in the Humboldt WEA from 2021/07/30 - 2021/08/04. Algorithm training was conducted on roughly one month of preceding data from the Morro Bay WEA. The confidence interval computed by GPR is shaded around the mean prediction function.

The 95% confidence interval (CI) calculated over the underlying functions of GPR is displayed in the second graph of Figure 7. The CI narrows around higher-confidence predictions, but is always non-zero due to the multitude of possible underlying functions and the inclusion of a noise kernel. The reliability of the regression is highly dependent on the selection of the covariance function, which must be specifically tuned to the nature of patterns in the target variable.

The first half of the displayed data in the GPR sample, where some of the observational data falls outside of the confidence interval, highlights important considerations to make when using GPR. The likely cause of the large deviation from observational data is a model limitation around capturing longer-term temporal trends. It is possible that the performance of RF and GPR in this instance could be improved by longer training time, or for GPR specifically, more trial-and-error fine-tuning of the kernel.

As discussed, the case-specific, iterative adjustments necessary to improve these two methods' prediction accuracies are a detriment to their overall usefulness for offshore wind modeling. However, it is important to consider the large distance

https://doi.org/10.5194/wes-2025-85
Preprint. Discussion started: 25 June 2025

between the ML training and testing sites in this study, which is 631 km (341 miles) between the Humboldt and Morro Bay WEAs. It is probable that model performance would greatly improve given a shorter distance between training and testing data locations, which would likely be the case in practical offshore wind energy applications of these models. Future studies employing these models across shorter train-test distances would help to quantify the prediction accuracy reduced by the large spatial extrapolation extent, but this is currently not possible with the limited available data.

3.1.3 ML Performance vs. Stability-Corrected Logarithmic Law

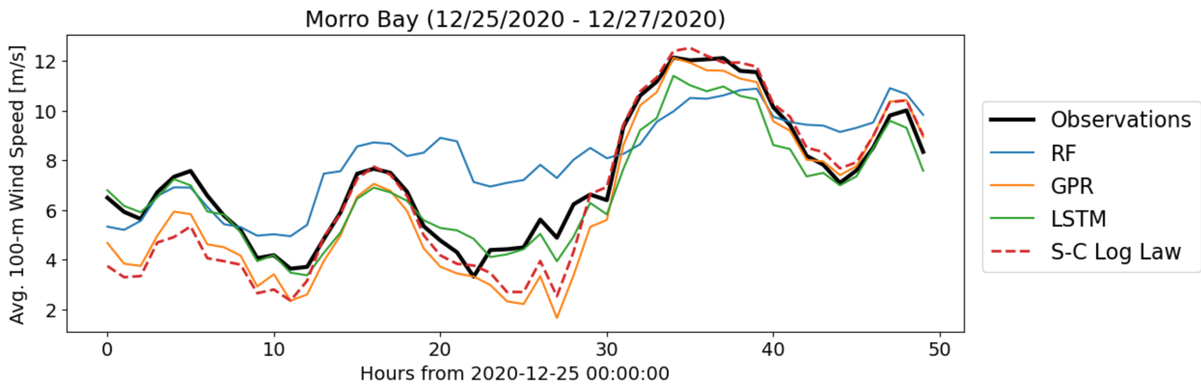

Figure 8. Sample comparison of ML predictions of 100-meter AMSL wind speeds versus values calculated from the Stability-Corrected Logarithmic Law. The testing data subset is from the Morro Bay WEA from 12/25/2020 to 12/27/2020. ML algorithm training was conducted on roughly one month of preceding data from the Humboldt WEA.

A comparison of the ML methods against the S-C log law on a slice of hourly Morro Bay test data from 2020/12/25 - 2020/12/27 is displayed in Figure 8. The S-C log law demonstrates similar performance to the ML techniques, and in some instances provides the most accurate comparison to the lidar data. Most similar in performance to the S-C log law are LSTM and GPR, which generally exhibit inaccuracies in conjunction with those of the S-C log law.

Figure 8 also illustrates an expected shortcoming of employing RF for wind energy purposes, which is smoothed predictions of stochastic wind speed extremes. Though the RF predictions respond to general wind speed pattern changes, the MAE from the RF predictions is highest for the majority of time points. This limitation can be attributed to the inherent process of regression tree averaging in RF, which makes the method robust to outlier data, but also less capable of accounting for anomalous wind events that may not be captured in the training data.

Hub-height wind speed prediction performance is generally assessed using bias, centered root mean squared error (cRMSE), square of correlation coefficient (R^2), and Earth-mover's distance (EMD) as the key performance metricsOptis et al. (2020). The decomposition of typical error metrics, such as root mean squared error (RMSE) and MAE, into more distinct components is useful for identifying specific aspects of each method's strengths and shortcomings, though RMSE is also taken into account

https://doi.org/10.5194/wes-2025-85
Preprint. Discussion started: 25 June 2025

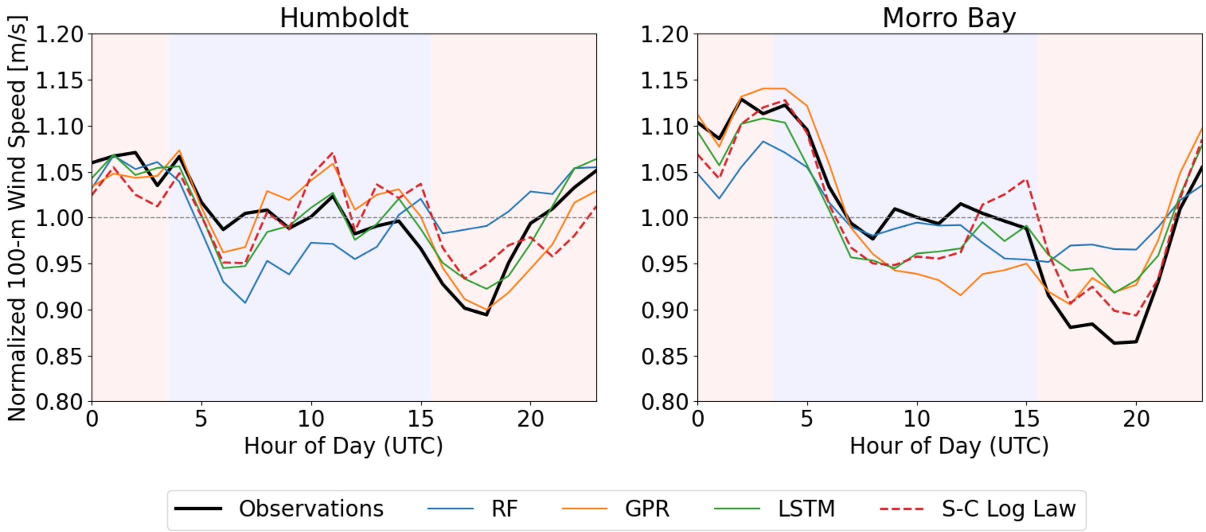

Figure 9. Comparison of observed and predicted diurnal averages of normalized 100-meter AMSL wind speed. The ML prediction data are only from runs using different train-test locations (i.e. the Humboldt predictions are made from a model trained on Morro Bay data, and vice versa). All averages are drawn from the times corresponding to the six sets of testing data, as detailed in Table 2. Red and blue background coloration indicates approximate daytime and nighttime conditions.

as a metric of overall prediction quality. The performance metrics of each prediction method are averaged over the 6 train-test datasets to obtain the compared values.

Figure 9 displays the average hourly 100-meter AMSL wind speed predictions across the diurnal cycle, with each prediction series normalized to the respective mean. The generalized offshore wind speed trend is again observable, with reductions induced by the more stable nighttime conditions beginning around 5 UTC and increased speeds brought about by convective daytime conditions beginning around 18 UTC.

The view of normalized wind speed per hour of the day elucidates some important aspects of ML model performance. RF demonstrates significant error across all parts of the diurnal cycle, as it tends to underestimate hub-height wind speeds in nighttime conditions and overestimates speeds in the daytime across both WEA locations. Individual model performances between the two locations appear to be relatively similar, which supports that the ML models' performances are not largely dependent on the particular training location in this study, lending confidence to the proficiency and applicability of each ML model's architecture.

The key performance metrics for each model are illustrated in the bar graphs in Figure 10. Table 5.3 in Chang (2022) also shows the average runtime of training and testing each algorithm over the six datasets. RF has the longest average runtime due to the computationally intensive process of training data subsetting and regression tree fitting. Though the number and depth of trees could be manually lowered to improve the runtime, prediction accuracy would likely degrade as a result. GPR delivers a moderate average runtime, likely on partial account of using only seven predictor variables and conducting dimensionality

https://doi.org/10.5194/wes-2025-85
Preprint. Discussion started: 25 June 2025

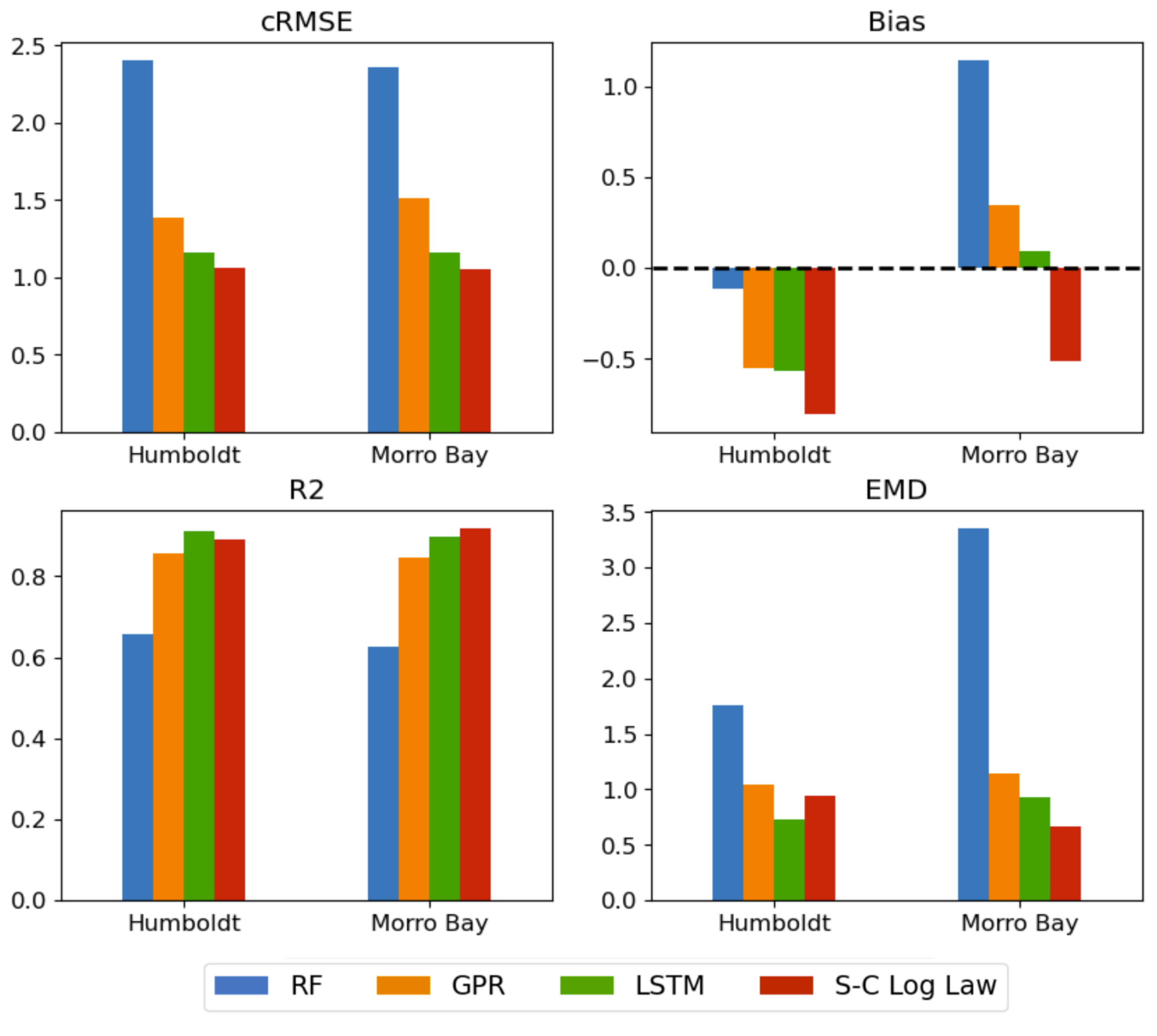

Figure 10. Site-specific error metrics of the ML methods' and the S-C log law's predictions of 100-meter AMSL wind speed. The ML prediction data shown are only from runs using different train-test locations.

https://doi.org/10.5194/wes-2025-85
Preprint. Discussion started: 25 June 2025

reduction on these variables with PCA. Training and testing of LSTM over the six datasets takes the shortest amount of time, averaging to just over two minutes in the case of this study.

Inferences made about RF performance from Figures 7, 8, and 9 are substantiated by the calculated error metrics. cRMSE, which represents unbiased model variation around the mean, is highest for RF in both locations and decreases in the order of GPR, LSTM, and S-C log law. The previously discussed samples of testing performance demonstrate the considerable prediction insufficiencies of RF for capturing stochastic wind speed variations. The R^2 values from RF indicate the poorest relative fit to the observed data, and values for EMD are the highest, evidencing a large difference between the predicted and actual probability distributions of 100-meter AMSL wind speed. Moreover, most of these RF error metrics do not substantially improve even when training and testing are conducted in the same location. Based on its many aspects of large prediction error, RF is deduced to be the least effective method for extrapolating Pacific OCS offshore hub-height wind speeds out of the techniques considered.

Relative to the four methods included in the study, GPR demonstrates average performance across the board, though its error metrics are much more similar in magnitude to those of LSTM and S-C log law than RF. Though the MSE of GPR is larger than that of LSTM and S-C log law, this aspect is countered by relatively lower overall prediction bias. GPR also demonstrates improvement in almost all performance metrics when trained on its same testing location and obtains an RMSE within ± 0.1 m/s of the S-C log law predictions. GPR is considered a promising method for Pacific OCS wind prediction for offshore energy purposes, especially notable for providing a confidence interval at every prediction timestep.

Wind speed predictions from LSTM are the most similar in cRMSE to the S-C log law and demonstrate smaller magnitudes of bias than the S-C log law. LSTM attains very similar performance metrics to the S-C log law in terms of cRMSE, R^2, and EMD. When trained and tested in the same location, LSTM produces more accurate wind speed results than the S-C log law for most of the error metrics considered. The LSTM results illuminate the importance of accounting for chronological wind sequence patterns and stochastic wind events within intelligent learning approaches to wind prediction. The performance of LSTM also highlights that additional training data or input variables are not necessarily imperative for attaining ML wind speed predictions similar or improved upon those calculated using the S-C log law. Considering the suboptimal spatial and temporal training data constraints, LSTM demonstrates very promising performance for Pacific OCS hub-height wind speed prediction and is recommended from the considered ML techniques for offshore wind speed extrapolation for wind energy purposes.

3.1.4 ML Train-Test Data Considerations

Training and testing in the same location generally improves ML prediction accuracy (see Table 5.3 in Chang (2022)). A sample of this ML performance improvement is shown in Figure 11, which displays a subset of hub-height wind speed predictions from December 2020. ML model training and testing in the same location (i.e. no spatial extrapolation) improves model RMSE in all cases except for the RF application to Humboldt data. Average RMSE decreases by 0.34 m/s for LSTM and by 0.49 m/s for GPR when the train-test location is the same. Without validation data available between the Humboldt and Morro Bay sites, it is uncertain how each ML model's prediction accuracy degrades as a function of distance from its training data location.

https://doi.org/10.5194/wes-2025-85
Preprint. Discussion started: 25 June 2025

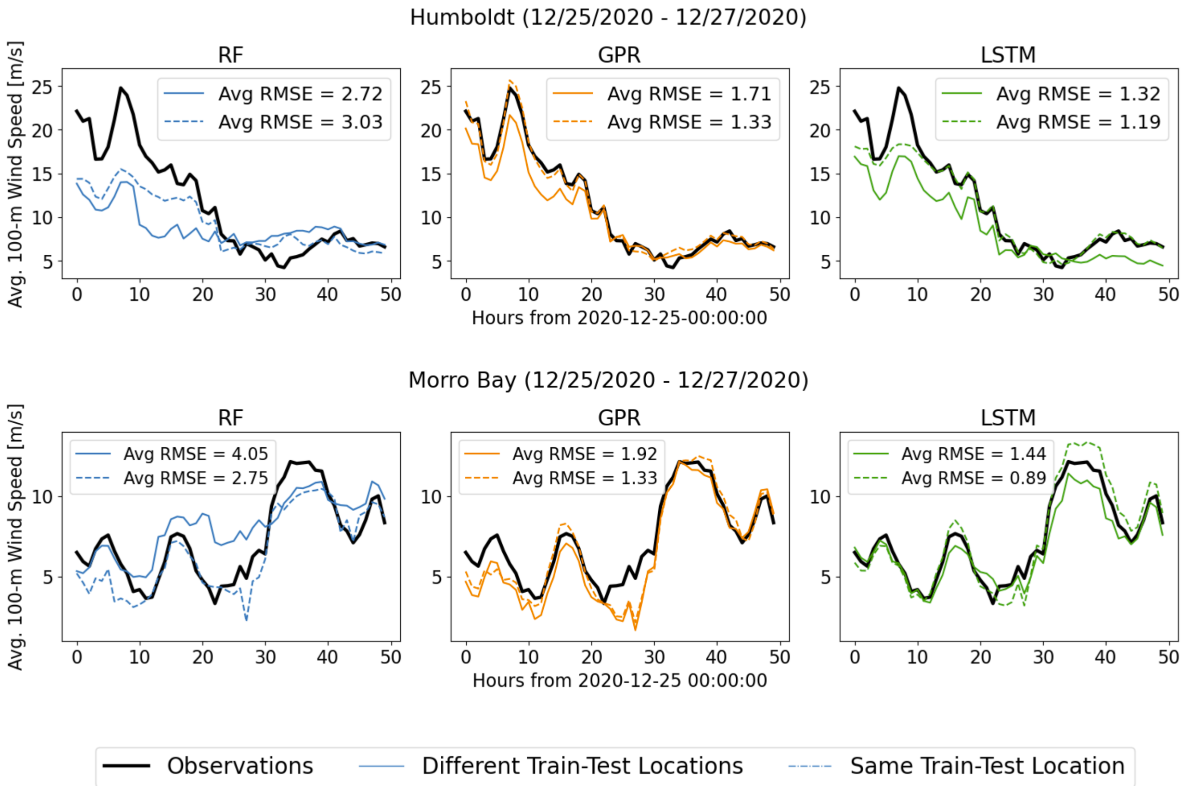

Figure 11. Differences in ML prediction performance of 100-meter AMSL wind speeds when using different train-test locations versus same train-test locations. "Avg RMSE" refers to the RMSE over all six testing datasets, not just the RMSE of the prediction subset shown.

In parallel to predictions made using different train-test locations, LSTM produces the most accurate wind speed predictions of the three ML algorithms in the same train-test site case. These conditions produce RMSE of 1.19 m/s and 0.89 m/s for the Humboldt and Morro Bay WEA locations respectively, which are the lowest RMSE values obtained from any prediction method used in this study, including the S-C log law. It is worth noting that these RMSE values are nontrivial; RMSE of 1 m/s still represents moderate error by wind energy industry standards. With this consideration in mind, the LSTM results still indicate high promise for using ML to generate accurate and site-specific wind speed predictions for future Pacific OCS offshore wind energy development. Even with the critical data constraints of this study, the LSTM performance metrics demonstrate that this technique is capable of producing turbine-height offshore wind speed predictions of similar or improved quality to those provided by the common and industry-standard S-C log law method, and additionally show that only readily-obtainable surface variables are needed as input data.

At the time of writing, a constraint presented by the DOE buoy data is the lack of continuous and complete lidar and surface variable data. The irregular data availability, caused by severe weather events and instrument failures, inhibits an in-depth analysis of each ML method's ability to account for interseasonal and interannual trends. With the buoy data available, the

https://doi.org/10.5194/wes-2025-85
Preprint. Discussion started: 25 June 2025

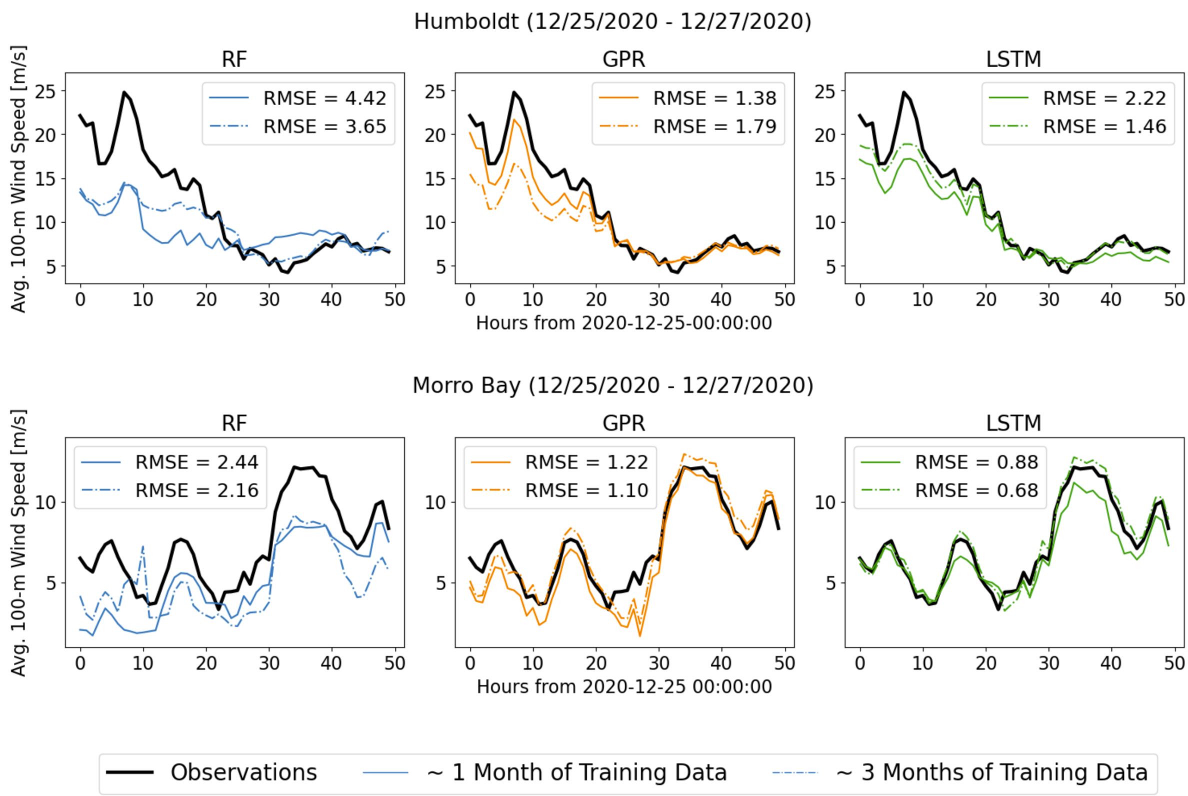

Figure 12. Differences in ML prediction performance of 100-meter AMSL wind speeds when using approximately one month of preceding training data versus approximately three months of preceding training data. The ML prediction data shown are only from runs using different train-test locations.

longest piece of continuous data in both locations runs from the beginning of October 2020 to near the end of December 2020. These three months of data provide an opportunity to test the effect of longer training data length. Figure 12 shows comparisons of approximately one month of training data (as is the case for all train-test datasets configured for this study) versus the approximate three months of training data, where both are tested on the same dates at the end of December.

In all cases except for the GPR-Humboldt predictions, using a longer training time effectuates moderate improvements in predictive accuracy. Though it was previously noted that additional training data is not imperative to obtain wind speed predictions similar to those of the S-C log law, this result further indicates the potential of the LSTM ML method to improve upon the predictive performance of the S-C log law given longer sequences of continuous training data.

3.1.5 Prediction Dependence on Atmospheric Stability

In Figure 13, model error metrics are categorized by the atmospheric stability condition during which each prediction was made. Across all prediction methods, stable conditions tend to produce the greatest prediction cRMSE and induce more model

https://doi.org/10.5194/wes-2025-85
Preprint. Discussion started: 25 June 2025

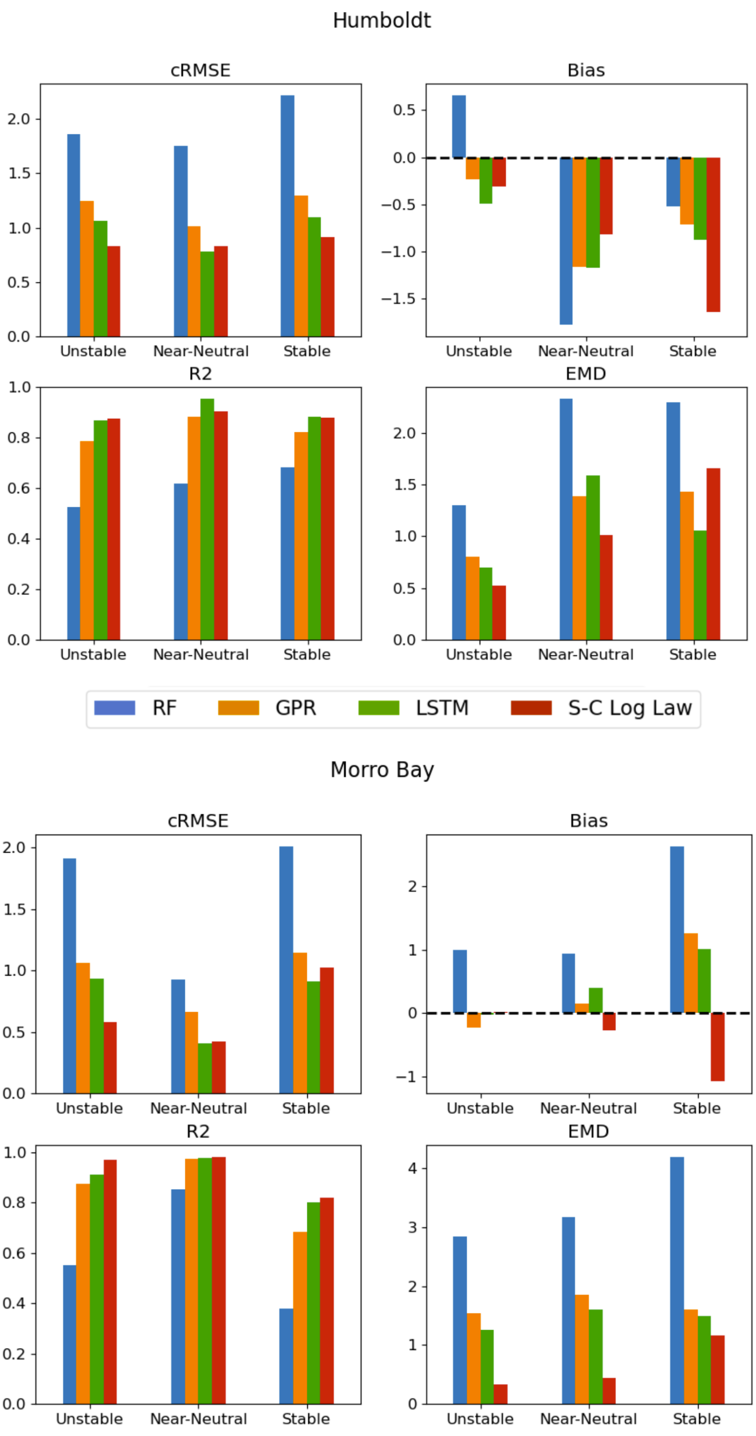

Figure 13. Error metrics of the ML methods' and the S-C log law's predictions of 100-meter AMSL wind speed, distinguished by the background atmospheric stability condition. The ML prediction data shown are only from runs using different train-test locations.

https://doi.org/10.5194/wes-2025-85
Preprint. Discussion started: 25 June 2025

bias, especially evident in the Morro Bay test data. A strong negative bias for stable conditions in Humboldt and positive biases across all ML algorithms for stable Morro Bay conditions suggests that shear profiles between the two locations may diverge under a stable regime. This inference is corroborated by the significant reduction of bias across all methods in unstable conditions.

The error magnitudes in RF and GPR lead to similar conclusions as above about the fidelity of each ML model's wind speed predictions. RF demonstrates the lowest R^2 and highest cRMSE and EMD across all regimes and remains the least accurate prediction method tested. GPR again performs between RF and LSTM across most error metrics, with exceptions of similar or lower bias compared to LSTM under unstable and near-neutral conditions. GPR is considered especially useful for its confidence estimates but is not currently recommended as a stand-alone method for Pacific OCS hub-height wind speed prediction.

The differences between Humboldt and Morro Bay metrics in Figure 13 present ambiguity in determining which method proves most robust to atmospheric stability conditions. LSTM and S-C log law both exhibit their lowest respective cRMSE under near-neutral conditions, in which both achieve values of less than 1 m/s in Humboldt and less than 0.5 m/s in Morro Bay. The cRMSE increases more for LSTM compared to S-C log law in unstable conditions. Comparative performance in terms of bias is inconclusive, as values do not show clear trends across the testing sites. S-C log law produces lower EMD values than LSTM (i.e. more similar probability distribution to the actual wind speeds) except for stable cases in Humboldt. In gross terms of performance metrics, S-C log law demonstrates a slight advantage over LSTM, but differences are not significant or consistent enough to substantiate a clear recommendation between the two methods based on atmospheric stability conditions.

3.1.6 Turbulence Intensity

Intelligent learning methods for wind speed prediction provide two inherent advantages over conventional physical law extrapolation techniques. Many of these intelligent methods are able to provide short-term forecasts; once trained, learned patterns can be extrapolated forward in time without additional inputs of training data Vassallo et al. (2020b). Though forecasting is outside the current scope of this study, it is a pertinent future research topic for Pacific OCS wind energy purposes. Additionally, these ML methods are not restricted to predicting vertically-extrapolated wind speeds, as are the S-C log law and power law estimates. Any environmental feature of interest can be predicted, with accuracy largely dependent on the skill of the ML model, the selection of predictor variables, and the natural correlation or stochasticity of the feature compared to the selected predictors.

For example, another important aspect of the wind resource to wind energy developers is turbulence intensity (TI), which represents the strength of wind velocity fluctuations. TI is important for assessing potential mechanical fatigue on wind turbines. TI calculations are influenced by ocean wave motion Gaudet et al. (2024), so algorithms that compensate for this could benefit from additional assistance from ML models. Due to lack of reference non-motion-impacted lidar TI observations, TI of 100-meter winds is gathered from the lidar buoy data by calculating the ratio of standard deviation of fluctuating wind velocity to the mean horizontal wind speed.

https://doi.org/10.5194/wes-2025-85
Preprint. Discussion started: 25 June 2025

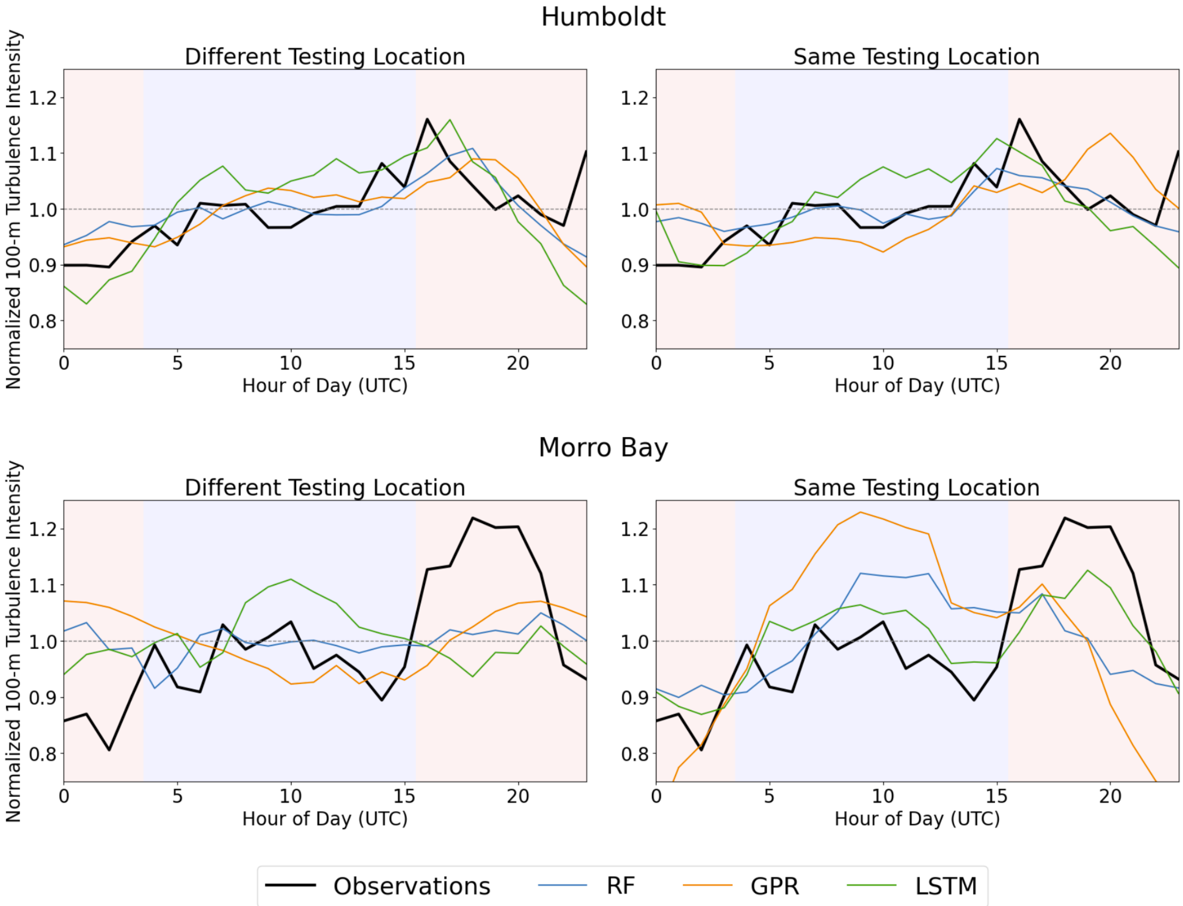

Figure 14. Comparison of observed and predicted diurnal averages of normalized 100-meter AMSL turbulence intensity (TI). All averages are drawn from the times corresponding to the six sets of testing data, as detailed in Table 4.3 of Chang (2022). Red and blue background coloration indicates approximate daytime and nighttime conditions.

https://doi.org/10.5194/wes-2025-85
Preprint. Discussion started: 25 June 2025

TI at 100 meters AMSL is predicted using the ML models following the same standard procedures as for 100-meter wind speed prediction. Results for normalized TI are displayed in Figure 14, and performance metrics are listed in Table 5.4 of Chang (2022). These procedures were tuned for prediction of wind speed and were not tested for relevance to patterns in TI; thus, results are not expected to be nearly as substantial as those for 100-meter wind speeds. Additionally, TI is quantified as a percentage, so the range of values is therefore more limited than for wind speed.

Patterns in TI are predicted to varying degrees of success between the ML algorithms and test locations. However, based on the generally low R^2 values, none of the prediction methods attain a significant degree of accuracy. This result is expected because of the lack of feature correlation analysis to TI and demonstrates the importance of surface variable examination and selection.

Despite the absence of model tuning and generally low prediction accuracy, similar trends to the 100-meter AMSL wind speed predictions emerge. LSTM predictions achieve the lowest RMSE and cRMSE for both the cases of same train-test location and for different train-test locations. Using the same train-test location again improves the majority of prediction error metrics across all models. The smallest RMSE value attained is from employing LSTM on the same train-test location data, for which it produces an RMSE of 6% across both sites. Overall prediction accuracy of the three ML algorithms, akin to the wind speed predictions, can be ranked as LSTM, GPR, and RF from highest to lowest proficiency. With further tuning of the ML models and input features, it is possible that one or more of these models could be capable of achieving accurate real-time TI estimates at turbine hub heights. This exploration of TI prediction emphasizes a primary advantage of employing machine learning methods for wind energy purposes, which is their adaptability for estimating parameters not otherwise obtainable by conventional physical law-based approaches.

https://doi.org/10.5194/wes-2025-85
Preprint. Discussion started: 25 June 2025

eawe european academy of wind energy
Open Access WIND ENERGY SCIENCE DISCUSSIONS

4 Conclusions

The three machine learning (ML) methods of random forest (RF), Gaussian process regression (GPR), and long short-term memory (LSTM) neural network were compared against the conventional stability-corrected logarithmic law (S-C log law) approach to assess predictive accuracy of hub-height wind speeds at two potential offshore wind sites. “Hub height" was generalized as 100 meters above mean sea level (AMSL) for this comparison and can be easily modified for similar future studies. The input predictor variables for ML model training were constrained to sea surface-elevation measurements in each offshore location, and opposite training and testing locations were used to prevent overfitting bias. The 631-km distance between the two locations in this study is likely relatively large compared to the practical future applications in the Pacific Outer Continental Shelf (OCS) wind energy industry; ML wind speed prediction performance can thus be considered as a general “lower limit" in this context.

Training and testing was conducted using six sets of data, each containing approximately one month of meteorological and oceanic data with hourly resolution averaged from 10-minute data. The predictor variables included in these datasets were initially analyzed for relevance to hub-height wind speed patterns and selected to be 4-meter AMSL wind speed, air temperature, sea surface temperature, air-sea temperature difference, atmospheric pressure, and time of day. Performance metrics for each method’s 100-meter AMSL wind speed predictions were obtained from average performance across the six train-test datasets. The best performance, generally evaluated from assessing the error metrics of bias, cRMSE, R^2, and EMD, were exhibited by LSTM and the S-C log law. RF produced the least accurate results and demonstrated notable insufficiencies in predicting stochastic or extreme wind speed events, likely due to its inherent prediction smoothing from regression tree averaging. GPR demonstrated slightly lower accuracy than LSTM and the S-C log law across most of the error metrics, though predictions were much more similar to these two methods than those from RF. Across all methods, stable atmospheric conditions tended to induce greater magnitudes of cRMSE and bias compared to neutral and unstable conditions. This result may be due to atypical shifts in the vertical wind shear profile influenced by stable stratification in the surface ABL.

It is important to note GPR’s advantage of providing empirical confidence intervals calculated inherently through its prediction method. The wind energy industry often requires uncertainty estimates to forecast different energy production scenarios. GPR is thus recommended as a promising method for offshore wind prediction but requires further study and model tuning.

The ML performance metrics were derived from predictions made over a 631 km train-test extrapolation distance. When trained and tested in the same location, LSTM surpassed the predictive performance of the S-C log law, while GPR was relatively similar to the S-C log law in terms of general predictive accuracy. Implementing a three month-long training time instead of one month similarly augmented prediction accuracy for almost all ML method test cases.

LSTM is demonstrated to be the most accurate and adaptable ML method for offshore wind speed prediction out of the techniques considered. Overall, the ML methods of LSTM and GPR present similar or improved offshore wind speed prediction performance compared to the conventional S-C log law technique in use by wind researchers and energy developers. In this study, these methods still present moderate prediction error by wind energy standards, and thus should not be used as validation data for other methods.

https://doi.org/10.5194/wes-2025-85
Preprint. Discussion started: 25 June 2025

ML methods offer greater flexibility for wind characterization than conventional physical law methods, as they can be used for predicting other wind parameters and can be used to make short-term forecasts. To demonstrate the former advantage, the 100-meter AMSL wind speed target variable was replaced with turbulence intensity (TI) at the same elevation. LSTM again demonstrated the highest prediction accuracy and RF the lowest, though general prediction accuracy of TI was significantly reduced compared to that of wind speed. TI prediction results could likely see significant improvements in future studies where predictor variables and model hyperparameters are specifically tuned with relevance to TI patterns.

Many possibilities exist for optimization of ML offshore wind speed prediction performance beyond this study. To amend the disparities in prediction performance across different atmospheric stability regimes, relevant predictor variables such as the Obukhov length L and surface TI could be included and compared against the original model runs. Other potentially relevant surface variables, including wind direction and relative humidity, were excluded from this study due to data irregularities or infidelity. Given continued data availability, more surface variables should be included in the train-test datasets and assessed for importance to model predictions. Additionally, though many ML hyperparameters were optimized through grid search tuning, some other hyperparameter values and functions were default selections and not tested for best suitability to wind speed prediction. A more thorough study of optimal ML hyperparameters in the context of offshore wind characterization would likely enhance the quality of the wind speed predictions.

The novel meteorological data being gathered in the Pacific OCS offshore environment offer plentiful opportunities for studying and modeling the Pacific offshore wind energy resource, but observational data are still extremely limited compared to most other wind energy development sites. Continued deployment of these scientific buoys on the Pacific OCS will help to amend the spatial and temporal constraints of the currently available data. With longer spans of continuous wind data, the discussed ML techniques could be trained across longer timescales and tested on their ability to capture interseasonal wind patterns. More spatial availability of observed vertical wind profiles between the Humboldt and Morro Bay WEAs would provide vital information for assessing the degradation of ML performance over shorter train-test extrapolation distances. Many more opportunities for wind energy ML method research are available through the possibilities for short-term forecasting and prediction of other wind parameters, such as wind power density and turbulence properties. Other important continuations of this research include drawing comparisons with wind prediction estimates from established numerical weather prediction models, and potentially combining individual ML techniques' predictive advantages through use of hybrid modeling.

The research presented determines that intelligent learning methods, namely LSTM and GPR, demonstrate new capabilities for providing accurate and adaptable predictions of offshore wind characteristics in comparison to conventional approaches. These state-of-the-art ML techniques can help inform the development of Pacific OCS offshore wind energy and potentially supplement the future research needed for other offshore wind energy projects.

Data availability. Humboldt Buoy surface data, https://doi.org/10.21947/1783807, Morro Bay Buoy surface data, https://doi.org/10.21947/1959715, Humboldt Buoy lidar data, https://doi.org/10.21947/1783809, Morro Bay Buoy lidar data, https://doi.org/10.21947/1959721.

https://doi.org/10.5194/wes-2025-85
Preprint. Discussion started: 25 June 2025

WIND ENERGY SCIENCE DISCUSSIONS

Author contributions. MFC conceptualized the work, designed methodology and software, performed formal analysis, and wrote the original draft. FKC and RK contributed to the methodology and formal analysis. FKC provided supervision and RK led the data curation. All authors reviewed and edited the manuscript. All authors contributed with critical feedback on this research and have read and agreed to the published version of the manuscript.

Competing interests. The authors declare that they have no conflict of interest.

Acknowledgements. Pacific Northwest National Laboratory (PNNL) is operated by Battelle Memorial Institute for the U.S. Department of Energy under Contract DE-AC05-76RL01830.

https://doi.org/10.5194/wes-2025-85
Preprint. Discussion started: 25 June 2025

References

Barthelmie, R., Badger, J., Pryor, S., Hasager, C., Christiansen, M., and Jørgensen, B.: Offshore Coastal Wind Speed Gradients: Issues for the Design and Development of Large Offshore Windfarms, Wind Engineering, 31, 369–382, https://doi.org/10.1260/030952407784079762, 2007.

Bodini, N. and Optis, M.: The importance of round-robin validation when assessing machine-learning-based vertical extrapolation of wind speeds, Wind Energy Science, 5, 489–501, https://doi.org/10.5194/wes-5-489-2020, 2020.

Bodini, N., Optis, M., Redfern, S., Rosencrans, D., Rybchuk, A., Lundquist, J. K., Pronk, V., Castagneri, S., Purkayastha, A., Draxl, C., Krishnamurthy, R., Young, E., Roberts, B., Rosenlieb, E., and Musial, W.: The 2023 National Offshore Wind data set (NOW-23), Earth System Science Data, 16, 1965–2006, https://doi.org/10.5194/essd-16-1965-2024, publisher: Copernicus GmbH, 2024.

BOEM: Humboldt Wind Energy Area | Bureau of Ocean Energy Management, https://www.boem.gov/renewable-energy/state-activities/humboldt-wind-energy-area, a.

BOEM: Morro Bay Wind Energy Area | Bureau of Ocean Energy Management, https://www.boem.gov/renewable-energy/state-activities/morro-bay-wind-energy-area, b.

BOEM: Outer continental shelf renewable energy, https://www.boem.gov/sites/default/files/documents/renewable-energy/2_Panel_ATL_Leases_WPAs_02_05_2025.pdf, 2025.

Chang, M. F.: Methods for Pacific OCS Wind Characterization for Offshore Wind Development, Ph.D. thesis, University of California, Berkeley, https://digicoll.lib.berkeley.edu/record/265596, 2022.

Crippa, P., Alifa, M., Bolster, D., Genton, M. G., and Castruccio, S.: A temporal model for vertical extrapolation of wind speed and wind energy assessment, Applied Energy, 301, 117 378, https://doi.org/10.1016/j.apenergy.2021.117378, 2021.

de Montera, L., Berger, H., Husson, R., Appelghem, P., Guerlou, L., and Fragoso, M.: High-resolution offshore wind resource assessment at turbine hub height with Sentinel-1 synthetic aperture radar (SAR) data and machine learning, Wind Energy Science, 7, 1441–1453, https://doi.org/10.5194/wes-7-1441-2022, publisher: Copernicus GmbH, 2022.

Dhiman, H. S. and Deb, D.: Machine Intelligent Techniques for Ramp Event Prediction in Offshore and Onshore Wind Farms, arXiv:2011.14220 [cs, eess], http://arxiv.org/abs/2011.14220, 2020.

DOE: Atmosphere to Electrons (A2e), https://doi.org/10.21947/1783809, 2021.

Edson, J. B., Jampana, V., Weller, R. A., Bigorre, S. P., Plueddemann, A. J., Fairall, C. W., Miller, S. D., Mahrt, L., Vickers, D., and Hersbach, H.: On the Exchange of Momentum over the Open Ocean, Journal of Physical Oceanography, https://doi.org/10.1175/JPO-D-12-0173.1, section: Journal of Physical Oceanography, 2013.

ESMAP: Offshore Wind Technical Potential \textbar Analysis and Maps, https://esmap.org/esmap_offshorewind_techpotential_analysis_maps.

Fairall, C. W., Bradley, E. F., Rogers, D. P., Edson, J. B., and Young, G. S.: Bulk parameterization of air-sea fluxes for Tropical Ocean-Global Atmosphere Coupled-Ocean Atmosphere Response Experiment, Journal of Geophysical Research: Oceans, 101, 3747–3764, https://doi.org/10.1029/95JC03205, _eprint: https://onlinelibrary.wiley.com/doi/pdf/10.1029/95JC03205, 1996.

Gaudet, B. J., Medina, G. G., Krishnamurthy, R., Sheridan, L. M., Yang, Z., Newsom, R. K., Pekour, M. S., Gustafson, W. I., and Liu, J.: Assessing Impacts of Waves on Hub-Height Winds off the U.S. West Coast Using Lidar Buoys and Coupled Modeling Approaches, Tech. Rep. PNNL-35856, Pacific Northwest National Laboratory (PNNL), Richland, WA (United States), https://doi.org/10.2172/2337529, 2024.

https://doi.org/10.5194/wes-2025-85
Preprint. Discussion started: 25 June 2025

Geernaert, G.: BOUNDARY LAYERS \textbar Surface Layer, in: Encyclopedia of Atmospheric Sciences, pp. 305–311, Elsevier, ISBN 978-0-12-227090-1, https://doi.org/10.1016/B0-12-227090-8/00092-0, 2003.

Golbazi, M. and Archer, C. L.: Surface roughness for offshore wind energy, Journal of Physics: Conference Series, 1452, 012 024, https://doi.org/10.1088/1742-6596/1452/1/012024, 2020.

Grachev, A. A. and Fairall, C. W.: Dependence of the Monin–Obukhov Stability Parameter on the Bulk Richardson Number over the Ocean, Journal of Applied Meteorology and Climatology, 36, 406–414, https://doi.org/10.1175/1520-0450(1997)036<0406:DOTMOS>2.0.CO;2, 1997.

Hasager, C. B., Madsen, P. H., Giebel, G., Réthoré, P.-E., Hansen, K. S., Badger, J., Pena Diaz, A., Volker, P., Badger, M., Karagali, I., Cutululis, N. A., Maule, P., Schepers, G., Wiggelinkhuizen, J., Cantero, E., Waldl, I., Anaya-Lara, O., Attya, A., Svendsen, H., Palomares, A., Palma, J., Gomes, V. C., Gottschall, J., Wolken-Möhlmann, G., Bastigkeit, I., Beck, H., Trujillo, J.-J., Barthelmie, R., Sieros, G., Chaviaropoulos, T., Vincent, P., Husson, R., and Prospathopoulos, J.: Design tool for offshore wind farm cluster planning: EWEA Annual Conference and Exhibition 2015, Proceedings of the EWEA Annual Event and Exhibition 2015, 2015.

Hochreiter, S. and Schmidhuber, J.: Long Short-Term Memory, Neural Computation, 9, 1735–1780, https://doi.org/10.1162/neco.1997.9.8.1735, 1997.

Jong, P. d., Dargaville, R., Silver, J., Utembe, S., Kiperstok, A., and Torres, E. A.: Forecasting high proportions of wind energy supplying the Brazilian Northeast electricity grid, Applied Energy, 195, 538–555, https://doi.org/10.1016/j.apenergy.2017.03.058, 2017.

Krishnamurthy, R., García Medina, G., Gaudet, B., Gustafson Jr., W. I., Kassianov, E. I., Liu, J., Newsom, R. K., Sheridan, L. M., and Mahon, A. M.: Year-long buoy-based observations of the air–sea transition zone off the US west coast, Earth System Science Data, 15, 5667–5699, https://doi.org/10.5194/essd-15-5667-2023, publisher: Copernicus GmbH, 2023.

Lange, B., Larsen, S., Højstrup, J., and Barthelmie, R.: Importance of thermal effects and sea surface roughness for offshore wind resource assessment, Journal of Wind Engineering and Industrial Aerodynamics, 92, 959–988, https://doi.org/10.1016/j.jweia.2004.05.005, 2004.

Liu, Y., Gaudet, B., Krishnamurthy, R., Tai, S.-L., Berg, L. K., Bodini, N., Rybchuk, A., and Kumler, A.: Identifying Meteorological Drivers for Errors in Modeled Winds along the Northern California Coast, Monthly Weather Review, https://doi.org/10.1175/MWR-D-23-0030.1, section: Monthly Weather Review, 2024.

Liu, Y., Juliano, T. W., Krishnamurthy, R., Gaudet, B. J., and Lee, J.: Linking large-scale weather patterns to observed and modeled turbine hub-height winds offshore of the US West Coast, Wind Energy Science, 10, 483–495, https://doi.org/10.5194/wes-10-483-2025, publisher: Copernicus GmbH, 2025.

Mahoney, W. P., Parks, K., Wiener, G., Liu, Y., Myers, W. L., Sun, J., Monache, L. D., Hopson, T., Johnson, D., and Haupt, S. E.: A Wind Power Forecasting System to Optimize Grid Integration, IEEE Transactions on Sustainable Energy, 3, 670–682, https://www.academia.edu/5099720/A_Wind_Power_Forecasting_System_to_Optimize_Grid_Integration, 2012.

McCoy, A., Musial, W., Hammond, R., Hernando, D. M., Duffy, P., Beiter, P., Pérez, P., Baranowski, R., Reber, G., and Spitsen, P.: Offshore Wind Market Report: 2024 Edition, Tech. Rep. NREL/TP-5000-90525, National Renewable Energy Laboratory, Golden, CO, 2024.

Moon, J., Park, S., Rho, S., and Hwang, E.: A comparative analysis of artificial neural network architectures for building energy consumption forecasting, International Journal of Distributed Sensor Networks, 15, 1550147719877 616, https://doi.org/10.1177/1550147719877616, 2019.

Optis, M., Bodini, N., Debnath, M., and Doubrawa, P.: Best Practices for the Validation of U.S. Offshore Wind Resource Models, Tech. Rep. NREL/TP-5000-78375, 1755697, MainId:32292, NREL, https://doi.org/10.2172/1755697, 2020.

https://doi.org/10.5194/wes-2025-85
Preprint. Discussion started: 25 June 2025

Optis, M., Bodini, N., Debnath, M., and Doubrawa, P.: New methods to improve the vertical extrapolation of near-surface offshore wind speeds, Wind Energy Science, 6, 935–948, https://doi.org/10.5194/wes-6-935-2021, publisher: Copernicus GmbH, 2021.

Ortega, C., Younes, A., Severy, M., Chamberlin, C., and Jacobson, A.: Resource and Load Compatibility Assessment of Wind Energy Offshore of Humboldt County, California, Energies, 13, 5707, https://doi.org/10.3390/en13215707, 2020.

Rasmussen, C. E. and Williams, C. K. I.: Gaussian processes for machine learning, Adaptive computation and machine learning, MIT Press, Cambridge, Mass., 3. print edn., ISBN 978-0-262-18253-9, 2008.

Release, D. P.: Biden-Harris Administration Advances Offshore Wind in the Pacific, https://www.doi.gov/pressreleases/biden-harris-administration-advances-offshore-wind-pacific, 2021.

Shao, B., Song, D., Bian, G., and Zhao, Y.: Wind Speed Forecast Based on the LSTM Neural Network Optimized by the Firework Algorithm, Advances in Materials Science and Engineering, 2021, e4874 757, https://doi.org/10.1155/2021/4874757, 2021.

Sheridan, L. M., Krishnamurthy, R., García Medina, G., Gaudet, B. J., Gustafson Jr., W. I., Mahon, A. M., Shaw, W. J., Newsom, R. K., Pekour, M., and Yang, Z.: Offshore reanalysis wind speed assessment across the wind turbine rotor layer off the United States Pacific coast, Wind Energy Science, 7, 2059–2084, https://doi.org/10.5194/wes-7-2059-2022, publisher: Copernicus GmbH, 2022.

Sheridan, L. M., Krishnamurthy, R., Gustafson Jr., W. I., Liu, Y., Gaudet, B. J., Bodini, N., Newsom, R. K., and Pekour, M.: Offshore low-level jet observations and model representation using lidar buoy data off the California coast, Wind Energy Science, 9, 741–758, https://doi.org/10.5194/wes-9-741-2024, publisher: Copernicus GmbH, 2024.

Taylor, P. K. and Yelland, M. J.: The Dependence of Sea Surface Roughness on the Height and Steepness of the Waves, Journal of Physical Oceanography, https://journals.ametsoc.org/view/journals/phoc/31/2/1520-0485_2001_031_0572_tdossr_2.0.co_2.xml, section: Journal of Physical Oceanography, 2001.

Vaisala: Wind Energy WindCube, https://www.vaisala.com/en/wind-lidars/wind-energy/windcube, publication Title: Vaisala.

Vassallo, D., Krishnamurthy, R., and Fernando, H. J. S.: Decreasing wind speed extrapolation error via domain-specific feature extraction and selection, Wind Energy Science, 5, 959–975, https://doi.org/10.5194/wes-5-959-2020, publisher: Copernicus GmbH, 2020a.

Vassallo, D., Krishnamurthy, R., Sherman, T., and Fernando, H. J. S.: Analysis of Random Forest Modeling Strategies for Multi-Step Wind Speed Forecasting, Energies, 13, 5488, https://doi.org/10.3390/en13205488, 2020b.

Wang, S. and Wang, S.: Impacts of wind energy on environment: A review, Renewable and Sustainable Energy Reviews, 49, 437–443, https://doi.org/10.1016/j.rser.2015.04.137, 2015.

Wieringa, J.: Updating the Davenport roughness classification, Journal of Wind Engineering and Industrial Aerodynamics, 41, 357–368, https://doi.org/10.1016/0167-6105(92)90434-C, 1992.

WWEA: WWEA Annual Report 2023: Record Year for Windpower, Tech. rep., World Wind Energy Association, https://wwindea.org/ss-uploads/media/2024/3/1711538106-40ab83f2-3e01-4c0a-9d28-e0a21bff72e6.pdf, 2024.